

Suppression of polarization decoherence for traveling light pulses via bang-bang dynamical decoupling

M. Lucamarini,^{1,2} G. Di Giuseppe,^{1,2} S. Damodarakurup,¹ D. Vitali,¹ and P. Tombesi^{1,2}

¹*School of Science and Technology, Physics Division, University of Camerino, via Madonna delle Carceri, 9, I-62032 Camerino (MC), Italy.*

²*CriptoCam s.r.l., via Madonna delle Carceri, 9, I-62032 Camerino (MC), Italy.*

(Dated: November 9, 2018)

In the propagation of optical pulses through dispersive media, the frequency degree of freedom acts as an effective decohering environment on the polarization state of the pulse. Here we discuss the application of open-loop dynamical-decoupling techniques for suppressing such a polarization decoherence in one-way communication channels. We describe in detail the experimental proof of principle of the “bang-bang” protection technique recently applied to flying qubits in [Damodarakurup *et al.*, Phys. Rev. Lett. **103**, 040502]. Bang-bang operations are implemented through appropriately oriented waveplates and dynamical decoupling is shown to be potentially useful to contrast a generic decoherence acting on polarization qubits propagating in dispersive media like, e.g., optical fibers.

PACS numbers: 03.67.Pp, 03.65.Yz, 42.25.Ja, 42.50.Ex

I. INTRODUCTION

The interest in the storage and manipulation of quantum systems have led the researchers to design strategies for preserving the coherence of such systems against the detrimental effects of the environment [1]. In fact, the uncontrollable degrees of freedom of the environment can get entangled with the quantum system and rapidly destroy the relative phase between the components of a linear superposition state.

Considerable efforts have been devoted to the issue of counteracting decoherence. Notable examples are quantum error-correction codes (QECC) [2–5] and decoherence-free subspaces (DFS) [6–8], both based on the careful encoding of the quantum state to be protected into a wider, partially redundant, Hilbert space (see Fig. 1). The drawback of these encoding strategies is the large amount of extra resources required [3]. Alternative approaches which avoid this hindrance have been developed and may be divided into two main categories: closed-loop control, also known as quantum feedback [9], and open-loop control [10–15] (see Fig. 1). In closed-loop techniques, the system to be protected is subject to appropriate measurements, whose results are then used for a real-time correction of the system dynamics. On the contrary, in open-loop controls, the system is subject to external, suitably tailored, time-dependent pulses which do not require any measurement. The control operations are chosen so that any undesired effect of the environment, such as dissipation, decoherence, heating, can be eliminated in principle if the controls are applied faster than the environment correlation time. The physical idea behind these open-loop schemes comes from refocusing techniques in NMR spectroscopy [16] where they are typically implemented via strong and rapid pulses known as “bang-bang” (BB) controls.

Open-loop decoupling strategies have been suggested in various physical contexts: to inhibit the decay of an

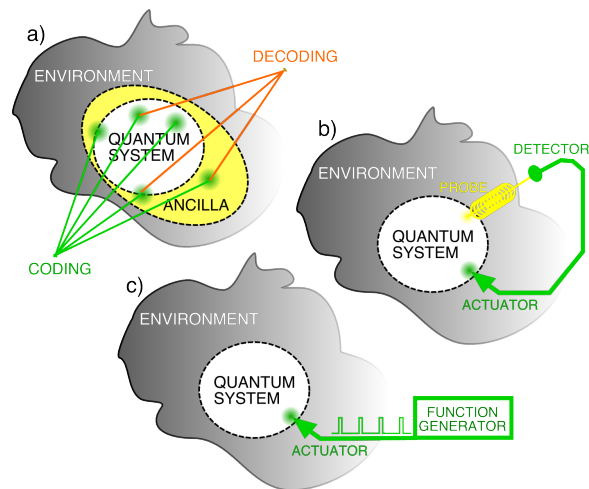


FIG. 1: (Color online) Strategies for protecting quantum system against decoherence: a) quantum error correction codes and decoherence-free subspaces, both based on state encoding; and a number of ancillary systems and on decoding techniques for retrieving the information; b) closed-loop techniques, based on measurements and consequent real-time correction of the system dynamics; c) open-loop controls, based on external, suitably tailored, time-dependent driving chosen such to eliminate undesired effect of the environment.

unstable atomic state [14, 17], to suppress the magnetic state decoherence [18] and the heating in ion traps [19], to contrast the quantum noise due to scattering processes [20] and the polarization mode dispersion [21] in optical fibers. BB control has been first demonstrated in NMR systems (see e.g. [22]). Then, it has been proven with nuclear spin qubits in fullerene [23], nuclear-quadrupole qubits [24] and very recently also with electron spins in Penning traps [25] and polarization qubits in a plane-parallel cavity [26] and in a ring cavity [27].

In this paper we discuss the last of the above-

mentioned applications [27] and provide an analytical explanation of the results. Photons interact very weakly with their environment and encoding quantum information in their polarization is a practical and convenient solution for many quantum communication protocols [28]. However, the optical properties of elements like mirrors, crystals and waveplates always depend upon both polarization and frequency, realizing in this way an effective coupling between the two degrees of freedom of the photon. The detection of the final polarization state is then performed by a detector that inevitably has a nonzero integration time. Hence the measurement traces out the frequency degree of freedom and if the field is not monochromatic all the information transferred to the frequency modes goes lost, inducing on the polarization qubit a dephasing process analogous to the “transversal” decay occurring in NMR.

Such a polarization decoherence can be inhibited by means of BB controls implemented in space, i.e., along the photon path, rather than in time, by means of suitably oriented waveplates. In Ref. [27] this idea is applied to the evolution of an optical pulse circling in a triangular ring cavity. Polarization decoherence occurs because of the reflection of the pulse on the cavity mirrors, which depend on both frequency and polarization. After a few cavity round trips, the initially pure polarization state becomes highly mixed. On the contrary, after inserting appropriate waveplates in the cavity realizing an effective impulsive BB, polarization decoherence is significantly inhibited.

Previously, a proof-of-principle of the BB impulsive dynamics was given in [26], by using optical pulses in a plane-parallel cavity. That experiment clearly demonstrates that BB can be applied to light pulses traveling back-and-forth between two points in space, e.g., on a two-way optical channel [29]. On the other hand, the present experiment including a ring cavity extends the applicability of BB to one-way channels, because it eliminates the need of a recycling mirror for suppressing decoherence, and relies entirely on BB impulsive controls.

The paper is organized as follows. In Sec. II we present a brief introduction on the dynamical decoupling. In Sec. III we describe the experimental apparatus of Ref. [27], i.e., the preparation of the input polarization state, the triangular ring cavity within which it propagates, and its final detection. We show how polarization decoherence emerges due to the polarization dispersive properties of the cavity mirrors. We also introduce the “compensated” cavity obtained by placing an additional \mathbb{Z} waveplate in the long arm of the cavity; this is needed if we require that the cavity induces a purely decohering dynamics on the pulse polarization. In Sec. IV we discuss a first experiment in which polarization decoherence is inhibited through the simple “Carr-Purcell” decoupling scheme [10, 11], which is a particular case of BB control realized by adding a single wave-plate within the cavity, suitably oriented. We then consider the more general Pauli-group decoupling [11], which is realized by

employing *two* waveplates with orthogonal rotation axes and we show that polarization decoherence is inhibited also in this case. Finally we modify our ring cavity setup in order to implement the most general form of decoherence acting on the polarization qubit. Generic qubit decoherence is realized by placing a Soleil-Babinet (SB) compensator with axis at 45° with respect to the cavity plane in front of each plane mirror. We show that, in accordance with theoretical predictions [11], Pauli-group decoupling is effective in inhibiting decoherence in this general case too. Sec. V is for concluding remarks.

II. THE “BANG-BANG”-CONTROL IDEA

The open-loop control technique takes advantage of the finite time of the relaxation process induced by the environment on the system. Accordingly, one is able to modify the dynamics by inducing motions on the system faster than the shortest time scale accessible by the environment.

For instance, to improve the resolution in NMR spectroscopy, multiple fast pulse sequences are used in order to reverse the effect of interactions of spins with the environment [30]. This is obtained through a careful tailoring of the amplitude, phase, and frequency of the time-dependent terms in the total Hamiltonian. The main example is the “spin echo” refocussing technique used in NMR, extensively investigated by E. L. Hahn [31], and later generalized by Carr and Purcell [32]. In that case, the main sources of noise are the inhomogeneities in the magnetic field and the molecular spin-spin interactions, which cause the total magnetization to dephase in a typical relaxation time called T_2 . At the microscopic level, the dephasing is due to the slightly different Larmor frequency experienced by each spin in the ensemble. In a reference frame which rotates about the z -axis at the Larmor frequency, the T_2 process can be visualized as the spreading of the magnetization vector in the transverse plane. One can then apply suitable RF pulses at the Larmor frequency to flip each spin by an angle of 180° . This realizes an effective “time reversal” for the molecules of the sample and leads, in the ideal case, to the rephasing of the magnetization vector.

This is analogous to what happens in a standard optical fiber because of the chromatic dispersion. When a light pulse travels in the fiber, all its components experience a different local birefringence, so they propagate at different velocities and the initial packet broadens. When a second fiber of opposite-sign dispersion is matched with the first one, a time-reversal of the frequency components occurs and the chromatic dispersion cancels out.

A general description of an open quantum system dynamical decoupling through open-loop control was given by Viola *et. al.* in Ref. [33]. Assuming a quantum system, S , described by the Hamiltonian H_S , plunged in an environment described by the Hamiltonian H_E , the total

Hamiltonian is given by:

$$H_0 = H_S \otimes \mathbb{I}_E + \mathbb{I}_E \otimes H_E + H_{SE}, \quad (1)$$

where H_{SE} represents the coupling between system and environment. The open-system properties like, e.g., the decoherence time, can be modified by adding to the system Hamiltonian a time-varying cyclic control, $H_c(t)$, with a period T_C such that

$$U_c(t) = \mathcal{T} \exp \left\{ -\frac{i}{\hbar} \int_0^t ds H_c(s) \right\} = U_c(t + T_C). \quad (2)$$

In this way the resulting dynamics of the quantum system, usually called ‘‘stroboscopic dynamics’’, is described by an effective Hamiltonian H_{eff} . If the period T_C is sufficiently shorter than the memory time of the environment, $1/\omega_C$, the effective Hamiltonian can be represented by the lowest-order average Hamiltonian [10]:

$$H_{eff} \sim \overline{H_0} = \frac{1}{T_C} \int_0^{T_C} dt [U_c^\dagger(t) H_0 U_c(t)]. \quad (3)$$

Corrections at higher orders in T_C can be systematically evaluated.

The simplest way of realizing a quantum system dynamical decoupling is through the quantum BB control, which operates by repeatedly applying instantaneous, arbitrarily strong, control pulses (‘‘kicks’’) to a qubit, thus disrupting the environmental interaction. This allows to convert the average over the cycle into a group-theoretic average, where a discrete set of unitary control operations, $\mathcal{G} = \{g_0, g_1, \dots, g_{|\mathcal{G}|-1}\}$, acting on the quantum system only, are introduced [13, 33]:

$$\overline{H_0} = \frac{1}{|\mathcal{G}|} \sum_{g_j \in |\mathcal{G}|} g_j^\dagger H_0 g_j. \quad (4)$$

Intuitively the BB symmetrizes the evolution with respect to the group \mathcal{G} , and the system is perfectly decoupled from the environment when the interaction with the environment is symmetrized to zero.

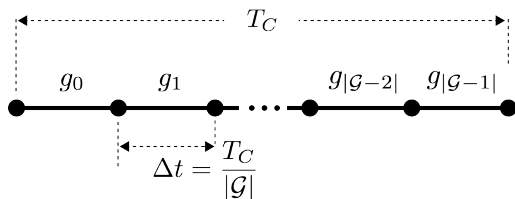


FIG. 2: Decoupling group control obtained by the symmetrization under the group \mathcal{G} .

Fig.2 provides a graphical representation of the BB idea. The quantum system enters from the left side and repeatedly undergoes the periodic transformations g_0 – $g_{|\mathcal{G}|-1}$. After each complete cycle in the group \mathcal{G} , the properties of the quantum system are restored to their initial value (up to corrections at the second order and

higher in $\omega_C T_C$). This allows, in principle, to indefinitely decouple the system from the environment.

At this point it is straightforward to figure out how the BB control can be adapted to the optical domain. A light pulse travels in a free-space portion of space or in an optical fiber and passes through a series of passive optical elements like waveplates or phase-shifters, disposed at regular intervals along the channel, in analogy to the schematics of Fig.2. Given the small thickness of the optical elements, the time employed by the light to pass through them is extremely small and well approximates the BB condition of instantaneous interaction.

A. Parity-kicks decoupling

In Ref. [12] it is showed how to inhibit decoherence through the application of shaped time-varying controls designed to be equivalent to the application of the parity operator on the system. The decoupling is realized by a sequence of very frequent ‘‘parity kicks’’ (PK) of duration τ_0 after a free evolution of duration Δt , $U(\Delta t) = \mathbb{U}_{\Delta t}$. Assuming that the external pulse is so strong that it is possible to neglect the free evolution during the pulse τ_0 , and that the pulse Hamiltonian H_k and the pulse width τ_0 can be chosen to satisfy the PK condition

$$U_k(\tau_0) \simeq e^{-\frac{i}{\hbar} H_k \tau_0} = \mathbb{P}, \quad (5)$$

the stroboscopic dynamics of the system inhibits decoherence whenever the following general conditions hold:

$$\mathbb{P} H_S \mathbb{P} = H_S \quad \mathbb{P} H_{SE} \mathbb{P} = -H_{SE}. \quad (6)$$

This means that the system Hamiltonian is parity invariant and the interaction with the external environment anticommutes with the system parity operator. Decoupling is then obtained through symmetrization with respect to the group

$$\mathcal{G} = \{\mathbb{I}, \mathbb{P}\}, \quad (7)$$

so that $|\mathcal{G}| = 2$. A harmonic oscillator with linear dissipation

$$H_{SE} = a^\dagger \Gamma + a \Gamma^\dagger, \quad (8)$$

satisfies such conditions, and the BB control is obtained by shifting the oscillation frequency ω_0 of $\delta\omega$ during the time τ_0 , under the constraint $\delta\omega \tau_0 = \pi$, for which $\mathbb{P} = \exp\{i\pi a^\dagger a\}$:

$$U_k^\dagger(\tau_0) \mathbb{U}_{\Delta t} U_k(\tau_0) \cdot \mathbb{I} \mathbb{U}_{\Delta t} \mathbb{I} \simeq \mathbb{P} \mathbb{U}_{\Delta t} \mathbb{P} \mathbb{U}_{\Delta t}. \quad (9)$$

PK control has a strong relationship with the spin-echo technique, because in both cases the applied pulses realize a time reversal of the unwanted Hamiltonian interaction and cancel its effect.

B. Carr–Purcell decoupling for \mathcal{H}^2 system

We consider now a particular system-environment interaction in which the decoherence occurs along a preferred axis, e.g., along z . In the standard spin-boson model this is described by the following interaction Hamiltonian:

$$H_{SE} = \sigma_z B_z. \quad (10)$$

Such an interaction can describe the above-mentioned pure dephasing process related to T_2 in NMR [34], when the magnetic field is aligned in the z direction, or the birefringence experienced by a light pulse traveling in a polarization-maintaining (PM) optical fiber with the fast axis parallel to the z direction. The “fast” and “slow” axes are the PM fiber eigenmodes. The pulses linearly polarized along the fast axis have a group velocity higher than those polarized along the slow axis. This implies that a pulse which is not polarized along one of these directions is split in two separate time bins with orthogonal polarizations. Such an effect must not be confused with the polarization-mode dispersion (PMD) of a single-mode (SM) optical fiber, which is mainly related to a non-perfect symmetry of the fiber core.

It is possible to use BB controls to reduce the decoherence induced by the interaction Hamiltonian of Eq.10. Following Ref. [21] a dynamical BB decoupling is realized by the repetition of only two steps: i) the free evolution of the system for an interval Δt represented by the unitary $U_{\Delta t}$; ii) the flip of the qubit around the x -axis through the operator \mathbb{X} . After two repetitions of these basic steps the system dynamics is driven by the following sequence of operators:

$$\mathbb{X} U_{\Delta t} \mathbb{X} U_{\Delta t} = U_{\Delta t}^\dagger U_{\Delta t} = \mathbb{I}, \quad (11)$$

where the first equality comes from the relation $\mathbb{X}Z\mathbb{X} = -Z$ and where $\mathbb{X} = \sigma_x$, $Z = \sigma_z$. The above sequence $U_{\Delta t}/\mathbb{X}$ defines a particular case of dynamical decoupling called “Carr–Purcell decoupling” (CP). When the interaction term is like in Eq.(10), i.e., when there is a preferred basis for decoherence to occur (the “pointer basis” [1]) then the CP alone is sufficient to decouple the system from the environment. More generally, the CP works perfectly when the noise acts along any axis orthogonal to the direction of the flip. Intuitively the spin-flip put forward by the \mathbb{X} operation changes the sign of the interaction Hamiltonian, Eq.(10), which is then symmetrized with respect to the group

$$\mathcal{G} = \{\mathbb{I}, \mathbb{X}\}. \quad (12)$$

This averages out the detrimental influence of the environment.

It is worthwhile to mention that the CP decoupling can be easily applied to PM fibers. It suffices to connect two PM fibers of equal length in a cross configuration, so that the fast axis of the first fiber is aligned to the

slow axis of the second. The cross-connector executes an operation analogous to the \mathbb{X} -flip just described, thus removing the difference in the group velocities due to the fiber birefringence.

C. General decoupling for \mathcal{H}^2 system

In the spin-boson model the most general interaction of a qubit with its environment is given by

$$H_{SE} = \sum_{\alpha=1}^3 \sigma_\alpha B_\alpha. \quad (13)$$

Decoherence acts along the axis parallel to the effective magnetic field B_α , which is however generally unknown. Therefore the simple CP-sequence is no more effective. Nonetheless decoupling can still be obtained through symmetrization with respect to the complete *Pauli group* PG:

$$\mathcal{G} = \{\mathbb{I}, \mathbb{X}, \mathbb{Y}, \mathbb{Z}\}, \quad (14)$$

with $(\mathbb{X}, \mathbb{Y}, \mathbb{Z}) = (\sigma_x, \sigma_y, \sigma_z)$ and $|\mathcal{G}| = 4$ [33, 35]. This can be implemented using only two spin-flips around two orthogonal axes, \mathbb{X} and \mathbb{Z} , because, apart an overall phase, we can write:

$$\begin{aligned} \mathbb{Z} U_{\Delta t} \mathbb{Z} \cdot \mathbb{Y} U_{\Delta t} \mathbb{Y} \cdot \mathbb{X} U_{\Delta t} \mathbb{X} \cdot \mathbb{I} U_{\Delta t} \mathbb{I} \\ = \mathbb{Z} U_{\Delta t} \mathbb{X} U_{\Delta t} \mathbb{Z} U_{\Delta t} \mathbb{X} U_{\Delta t}. \end{aligned} \quad (15)$$

With PG is possible to decouple the system from the environment, whatever the direction of the interaction Hamiltonian, up to the first order in $\omega_C T_C$ [21, 33, 35]. However it is worth to notice that more general decoupling schemes are possible which achieve decoupling at higher orders in $\omega_C T_C$ [36].

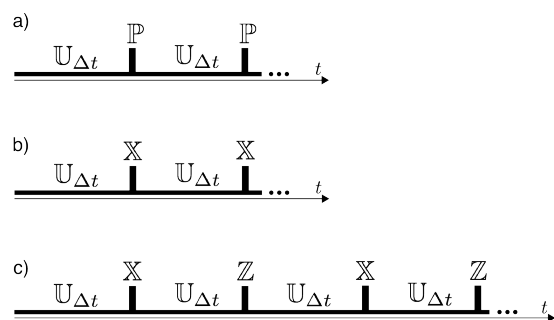


FIG. 3: Decoupling BB cycles for: a) parity-kicks (PK); b) Carr–Purcell (CP); c) Pauli group.

Fig.3 summarizes the open-loop decoupling techniques described so far, in the BB approximation of instantaneous control pulses. The inset (a) and (b) of the figure contain the schematics of PK and CP decoupling techniques respectively; their use in the optical domain has already been discussed. The inset (c) represents the most

general decoupling scheme, the PG. It becomes particularly important when the preferred axis of the system-environment interaction is unknown, e.g., in an SM optical fiber. In fact, it is possible to segment an SM fiber into smaller and smaller portions until a unity of length L_0 is reached which features a constant birefringence (along unknown axes) and so constant dispersive properties. Regardless of the direction of the birefringence, PG decoupling can be applied on a length scale comparable to L_0 to suppress decoherence on each segment of the SM fiber and, by consequence, on the fiber as a whole.

D. Decoherence for polarization-qubits

All of the described decoupling scheme, in particular the PG, are suitable for a straightforward application in the optical domain. Photons are ideal carriers of quantum information as they allow a fast transfer of information while interacting weakly with the surroundings. However in the practice photons are replaced by light pulses which are intrinsically non-monochromatic and are measured by detectors which do not possess an infinite integration time. Hence, a vast part of the information committed to the frequency degree of freedom is traced out by the final measuring process, which is not able to discriminate each frequency component of the light pulse.

A solution to this problem is to encode information in the polarization degree of freedom. However, when the light propagates in a dispersive medium, such as an optical fiber, the initial information can spread out to other unwanted degrees of freedom, like frequency, and again that information will go lost. So in this case the frequency degree of freedom acts as the environment of the polarization qubit and induces a dephasing process on it.

This happens because the dispersive medium couples the two degrees of freedom with an interaction Hamiltonian like the following:

$$H_{SE} = \sum_{\alpha=1}^3 \sigma_{\alpha} n_{\alpha}(\omega), \quad (16)$$

where $n_{\alpha}(\omega)$ is the frequency-dependent refractive index of the medium and σ_{α} are the generators of the polarization-qubit evolution. The above Hamiltonian descends from the Fourier transform of the one describing a light pulse propagating in an inhomogeneous medium, i.e. with an index of refraction that depends on the position of the pulse. So it is closely related to the above-mentioned PMD occurring in SM optical fibers. The similarity with Eq.(13) is apparent; this means that PG can be employed to adverse the polarization decoherence due to PMD. In a classical communication scenario PMD adversely affect the rate of long distance communications [37, 38]. PMD is also substantial in a fiber-based quantum communication if one uses a qubit realized in polarization since the unavoidable coupling with

the birefringent environment affect the purity and fidelity of transmitted qubits [39]

There are not many techniques to combat the PMD detrimental effects. One is of course to adopt a PM fiber, but it works only for the two linear polarizations aligned to the fiber eigenmodes. Another technological solution is to spin the SM fiber so to distribute inhomogeneities symmetrically in the core [40]; however this increases the fiber attenuation more than 20 times for wavelengths in the third Telecom window. Finally, one solution is based on Faraday mirrors [26, 29]. The principle is that of “retracing beam”: a light pulse travels back and forth along the communication channel; this leads it to compensate during the backward travel all the PMD encountered in the forward travel. The only assumption in this case is that the PMD remains constant during the two trips of the pulse [29]. This technique is clearly not applicable to all those channels where the information carriers travel in the forward direction only.

Given the lack of conclusive solutions to adverse the PMD on one-way communication channels, it is quite surprising that BB dynamical decoupling has not been already applied to the optical domain. In fact specific experiments on this subject are missing. The remarkable experiments reported in [26] cannot be deemed an exception in this respect, since they partly rely on the principle of retracing beam; so their application appears to be more suitable for two-way communication channels. In the following we focus on the recent demonstration given in [27] and show the effectiveness of the BB dynamical decoupling for suppressing the decoherence of a polarization qubit confined in a *ring cavity*. The choice of a ring cavity has a twofold motivation: on one side it realizes the Hamiltonian of Eq.(16), which well mimic the effect of PMD in a dispersive medium. The second reason is that a ring cavity represents the perfect simulation of a one-way channel: the principle of retracing beam is removed as its root because errors tend to accumulate rather than to cancel out.

III. THE EXPERIMENTAL SETUP AND ITS CHARACTERIZATION

The experimental apparatus of Ref.[27] is depicted in Fig. 4. A laser diode with central wavelength at $\lambda_0 \simeq 800$ nm and bandwidth $\Delta\lambda \simeq 15$ nm is pulsed at repetition rate of 100 KHz and pulse duration ~ 100 ps. The laser is attenuated and injected in a triangular ring cavity through a spherical mirror. The polarization state of the laser is prepared by using a polarizing beam-splitter (PBS), a half-wave plate ($\lambda/2$) and a quarter-wave plate ($\lambda/4$) with a very high degree of purity. At every round trip the light is extracted from the cavity with 4% probability using a ~ 100 μm thin glass plate. Its polarization is analyzed by means of the tomographic technique [41], and then sent into a multimode fiber connected to a single-photon detector with quantum efficiency $\sim 70\%$.

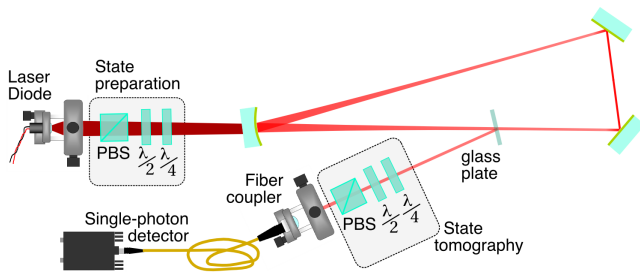


FIG. 4: (Color online) Schematics of the experimental apparatus. The polarization of pulsed laser diode is determined by a state preparation apparatus, which is constituted by a polarizing beam-splitter (PBS), a half-wave plate ($\lambda/2$) and a quarter-waveplate ($\lambda/4$). The laser pulses are attenuated and injected in a triangular-ring cavity constituted by a spherical mirror and two plane mirrors at 45° . The pulses trapped in the cavity are extracted by means of a glass plate and sent into the state tomography apparatus constituted by a PBS, $\lambda/2$ and $\lambda/4$. The light is finally coupled to an optical fiber and detected by a single-photon avalanche photodiode.

Let us now separately discuss the generation, processing, and measurement of the qubit.

A. Operational polarization qubit

The attenuated pulse entering the cavity through the input spherical mirror and after the state preparation stage can be well described as a multi-mode weak coherent state, which can be written as

$$|\psi\rangle_{in} = \exp \left\{ \int d\omega [\alpha_H(\omega)\hat{a}_H(\omega)^\dagger + \alpha_V(\omega)\hat{a}_V(\omega)^\dagger \pm H.C.] \right\} |vac\rangle. \quad (17)$$

$\hat{a}_S(\omega)^\dagger$ is the operator creating a photon with polarization $S = \{H, V\}$ and frequency ω , satisfying the commutation relation $[\hat{a}_S(\omega), \hat{a}_{S'}(\omega')^\dagger] = \delta_{S,S'}\delta(\omega - \omega')$, and $|vac\rangle$ denotes the vacuum state. We denote with V (H) the polarization orthogonal (parallel) to the plane of the cavity.

The polarization of the pulse is fully characterized by its Stokes parameters, which are determined by the functions $\alpha_H(\omega)$ and $\alpha_V(\omega)$ according to

$$s_0 = \int d\omega [|\alpha_H(\omega)|^2 + |\alpha_V(\omega)|^2], \quad (18)$$

$$s_1 = \int d\omega [|\alpha_H(\omega)|^2 - |\alpha_V(\omega)|^2], \quad (19)$$

$$s_2 = \int d\omega [\alpha_H(\omega)^*\alpha_V(\omega) + \alpha_H(\omega)\alpha_V(\omega)^*], \quad (20)$$

$$s_3 = -i \int d\omega [\alpha_H(\omega)^*\alpha_V(\omega) - \alpha_H(\omega)\alpha_V(\omega)^*]. \quad (21)$$

One can associate to the full state of the field of Eq. (17) a polarization state described by the 2×2 qubit density

matrix

$$\rho_{pol} = \frac{1}{2}(1 + \vec{P} \cdot \vec{\sigma}), \quad (22)$$

where $\vec{\sigma} = (\mathbb{X}, \mathbb{Y}, \mathbb{Z})^T$ is the vector of the three Pauli matrices, and $\vec{P} = (s_2/s_0, s_3/s_0, s_1/s_0)^T$ is the Bloch vector, completely characterizing the state of the polarization qubit. The Stokes parameters of Eqs. (18)-(21) satisfy the condition $s_0^2 - s_1^2 - s_2^2 - s_3^2 \geq 0$, which is equivalent to the condition on the Bloch vector norm $|\vec{P}| \leq 1$, which is required by the fact that ρ_{pol} must describe a physical density matrix. This condition can be verified using the fact that Eqs. (18)-(21) imply

$$\begin{aligned} s_0^2 - s_1^2 - s_2^2 - s_3^2 \\ = \int \int d\omega d\omega' |\alpha_H(\omega)\alpha_V(\omega') - \alpha_H(\omega')\alpha_V(\omega)|^2 \geq 0. \end{aligned} \quad (23)$$

Notice that this latter equation shows that the inequality becomes an equality, i.e., $|\vec{P}| = 1$ and the polarization state is a pure qubit state, if and only if $\alpha_H(\omega)\alpha_V(\omega') = \alpha_H(\omega')\alpha_V(\omega)$, $\forall \omega, \omega'$, which is realized if and only if the ratio $\alpha_H(\omega)/\alpha_V(\omega)$ does not depend upon ω . This is verified when the polarization state of the pulse is independent of its frequency distribution, i.e., polarization and frequency are factorized and one can write $\alpha_S(\omega) = \epsilon(\omega)\alpha_S$ ($S = H, V$). Therefore for the multi-mode coherent state of Eq. (17), the polarization state ρ_{pol} is pure if and only if is “disentangled” from the frequency $\alpha_S(\omega) = \mathcal{E}(\omega)\alpha_S$ ($S = H, V$), with $\mathcal{E}(\omega)$ the amplitude spectrum of the pulse normalized such that $\int d\mu_\omega \equiv \int d\omega |\mathcal{E}(\omega)|^2 = 1$, and in this case it is represented by a frequency-independent Jones vector

$$|\pi\rangle_{in} = \frac{1}{\sqrt{|\alpha_H|^2 + |\alpha_V|^2}} \begin{pmatrix} \alpha_H \\ \alpha_V \end{pmatrix}. \quad (24)$$

On the contrary, if $\alpha_H(\omega)/\alpha_V(\omega)$ depends upon ω , the Jones vector is frequency-dependent, and ρ_{pol} is mixed: polarization and frequency are effectively “entangled”.

The weak coherent pulse is then injected into the cavity, where it is transformed by the action of mirrors, which are linear and passive elements and therefore can only mix $\hat{a}_H(\omega)^\dagger$ and $\hat{a}_V(\omega)^\dagger$, without involving processes like creation or annihilations of photons. Also the additional elements which will be later added within the cavity for the realization of the BB control, i.e., waveplates and Soleil-Babinet(S-B) compensators, are linear and passive devices, and therefore the action of a generic element within the cavity can always be described in terms of a 2×2 unitary matrix form. The overall transformation for each round-trip in the cavity is given by:

$$\begin{bmatrix} \hat{a}_H(\omega)^\dagger \\ \hat{a}_V(\omega)^\dagger \end{bmatrix} \rightarrow \mathbf{U}(\omega) \begin{bmatrix} \hat{a}_H(\omega)^\dagger \\ \hat{a}_V(\omega)^\dagger \end{bmatrix}, \quad (25)$$

and the coherent state pulse is changed into

$$|\psi\rangle_{tr} = \exp \left\{ \int d\omega [\beta_H(\omega)\hat{a}_H(\omega)^\dagger + \beta_V(\omega)\hat{a}_V(\omega)^\dagger \pm H.C.] \right\} |vac\rangle, \quad (26)$$

where

$$\begin{pmatrix} \beta_H(\omega) \\ \beta_V(\omega)^\dagger \end{pmatrix} = \mathbb{U}(\omega)^T \begin{pmatrix} \alpha_H(\omega) \\ \alpha_V(\omega) \end{pmatrix}. \quad (27)$$

The Stokes parameters and consequently the polarization state is changed accordingly.

The final attenuator (in the experimental setup the glass plate), η , decreases the intensity of the pulse, $\beta_S(\omega) \rightarrow \eta\beta_S(\omega)$ with $\eta \ll 1$. Assuming $\eta^2 \int d\omega |\beta_S(\omega)|^2 \ll 1$, the state of the pulse at the cavity output and just at the entrance of the detection stage can be well approximated by the first order linear expansion of the exponential in Eq. (26)

$$|\psi\rangle_{tr} \simeq |vac\rangle + \eta \int d\omega [\beta_H(\omega)\hat{a}_H(\omega)^\dagger + \beta_V(\omega)\hat{a}_V(\omega)^\dagger] |vac\rangle. \quad (28)$$

By post-selecting the events with at least one photon we discard the vacuum component and the state entering the detector is well approximated by a single-photon state given by the integral term on the right hand side of Eq. (28).

One issue that should be addressed is the use of the term ‘‘polarization qubit’’ for the description of the laser pulse traveling in the ring cavity just described. If the frequency distribution is independent of the polarization, one can write $\beta_S(\omega) = \mathcal{E}(\omega)\beta_S$ ($S = H, V$), and factorize the frequency and polarization degree of freedom

$$|\psi\rangle_{out} \simeq \int d\omega \mathcal{E}(\omega)|\omega\rangle [\beta_H|H\rangle + \beta_V|V\rangle]. \quad (29)$$

If instead the polarization state is not independent of the frequency, the two degrees of freedom are entangled and one has decoherence when one looks at the polarization state only. What is relevant is that the Bloch vector \vec{P} and therefore the polarization state is not changed by the extraction by the glass plate, and, obviously, by the post-selection as well. Therefore the output single photon state, ‘‘operational’’ polarization qubit, perfectly describes the polarization state within the cavity, even if we have a coherent state pulse within the optical system with a non-zero probability of having more than one photon.

In our experiment the state emerging from the laser is a coherent state with average photon number per pulse about equal to 1 soon after the mirror. The resulting coherent state entering the detection apparatus has a mean photon number per pulse $\mu \leq 4 \times 10^{-2}$, and the probability of having two or more photons in a detection event is less than 2%, as we have experimentally verified. The experimental setup detailed above then justifies a description in terms of single-photon polarization qubits, and allows us to write the state injected into the cavity, soon after the spherical mirror, as an effective single-photon state

$$|\psi\rangle_{in}^{\text{eff}} = \int d\omega \mathcal{E}(\omega)|\omega\rangle \otimes |\pi\rangle_{in}, \quad (30)$$

where $|\omega\rangle \otimes |\pi\rangle_{in} = [\alpha_H\hat{a}_H(\omega)^\dagger + \alpha_V\hat{a}_V(\omega)^\dagger]|0\rangle$.

B. The cavity

The triangular ring cavity (see Fig. 5) is realized by a spherical mirror with radius of curvature 1 m and reflectivity $\sim 98\%$. The cavity is also formed by two flat mirrors at 45° with reflectivity $\gtrsim 99\%$. The aperture angle of the cavity at the spherical mirror is $\sim 8^\circ$. The long arms of the cavity are ~ 0.94 m and the short arm is ~ 0.13 m determining a total cavity length of ~ 2.01 m. A cavity

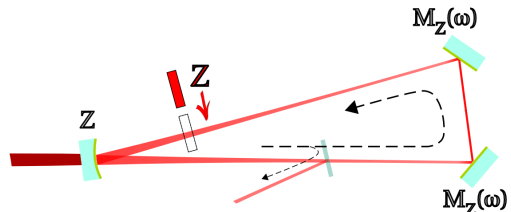


FIG. 5: (Color online) Schematics of the triangular-ring cavity constituted by a spherical mirror and two plane mirrors at 45° , which realize on the polarization a unitary operation, \mathbb{Z} , and a frequency dependent unitary operations, $\mathbb{M}_Z(\omega)$, respectively. A wave-plate inserted in a long arm of the cavity implements the \mathbb{Z} operation in order to compensate for the spherical mirror \mathbb{Z} transformation.

mirror generally produces a phase shift which depends upon both frequency and polarization, and therefore its action is described by the matrix [42] (keeping always the right-hand coordinate system before and after reflection [43, 44])

$$\mathbb{M}_Z(\omega) = \begin{bmatrix} e^{-i\phi_H(\omega)} & 0 \\ 0 & e^{-i\phi_V(\omega)+i\pi} \end{bmatrix} = \mathbb{Z} \exp\{-i\phi(\omega)\mathbb{Z}\}, \quad (31)$$

where we have omitted an unessential global phase factor and we have defined with $\phi(\omega) = \phi_H(\omega) - \phi_V(\omega)$ the relative phase due to the polarization-reflectivity difference. This is due to the different reflection coefficients for orthogonal and parallel polarizations with respect to the plane of the cavity (s- and p- polarization, respectively). The two plane mirrors at 45° can be assumed identical and are therefore characterized by the same matrix $\mathbb{M}_Z(\omega)$. The third concave mirror of the cavity is almost at normal incidence: this mirror does not distinguish H and V polarization, so that $\phi(\omega) \simeq 0$ and therefore it acts as $\mathbb{M}_Z(\omega) \simeq \mathbb{Z}$. The polarization qubit in the cavity is subjected to a phase-noise along z -axis and the unitary operator describing the polarization transformation after one cavity round-trip for a given frequency component is given by

$$\begin{aligned} \mathbb{U}[\phi(\omega)] &= \mathbb{Z} \cdot \mathbb{M}_Z(\omega) \cdot \mathbb{M}_Z(\omega) \\ &= \mathbb{Z} \exp\{-i2\phi(\omega)\mathbb{Z}\}, \end{aligned} \quad (32)$$

The dispersive properties of the two plane mirrors at 45° , i.e., their frequency dependence, generates polarization decoherence: in fact the frequency dependence of the matrix \mathbb{M}_Z appears only if the optical element is dispersive,

otherwise it is constant and it does not entangle polarization and frequency degrees of freedom.

C. State tomography reconstruction

At every round trip the light is extracted from the cavity using the thin glass plate as shown in the setup of Figs. 4 and 5. The output polarization state after n round-trips is given by the reduced density matrix obtained by tracing over the frequency degree of freedom

$$\hat{\rho}_{out}^{(n)} = \int d\mu_\omega \mathbb{U}[\phi(\omega)]^n |\pi\rangle_{in} \langle \pi| \mathbb{U}^\dagger[\phi(\omega)]^n. \quad (33)$$

Experimentally the output density matrix after n round-trips has been evaluated by the acquisition of the output signal from the detector, which stops the time conversion in a Time-to-Amplitude Converter (TAC) synchronized with the laser. The time delay between the input and output signals is then recorded by a Multi-Channel Analyzer (MCA) with a resolution of 8192 channels. The acquisition electronics has a time-resolution of 102 ps. Typical acquisition runs are shown in Fig. 6, showing a sequence of peaks, each corresponding to a cavity round-trip. The interval between adjacent peaks amounts to ~ 6.80 ns, in agreement with the measured length of the cavity. In all the experiments both the decoherence and the effect of BB control are studied by sending specific input polarization in the cavity and capturing the photon round trip from the cavity with respect to different tomographic measurement bases. Fig. 6 depicts the photon round trips for *horizontal* (H), *diagonal* (D), and *right* (R) polarization with respect to \mathbb{Z} , \mathbb{X} and \mathbb{Y} basis tomographic measurement. The decay of peaks after every round trip for H polarization input state is highly uniform with respect to all basis measurements but for D and R polarizations it is highly non-uniform, indicate that the eigenstates of the cavity unitary evolution are H and V *vertical* polarizations.

This is made evident by the time evolution of the Stokes parameters for D and R input polarization rates, as shown by the left panels in Fig. 7. The Stokes' parameters are calculated as expectation values of the Pauli matrices ($\sigma_z, \sigma_x, \sigma_y$) over the density matrices evaluated by maximum-likelihood optimization procedure [41] on the six experimental counts obtained by integration of ten time bins around each peak for the three polarization measurement bases.

A numerical simulation of Eq. (33) has been run assuming a Gaussian frequency spectrum for the input pulse given by

$$\mathcal{E}(\omega) = \frac{1}{\sqrt{4\pi\sigma_\omega^2}} \exp[-(\omega - \omega_0)^2/2\sigma_\omega^2], \quad (34)$$

where σ_ω represents the bandwidth of the radiation spectrum centered in ω_0 . The frequency dependence of the integrand is determined by the fact that, with a very good

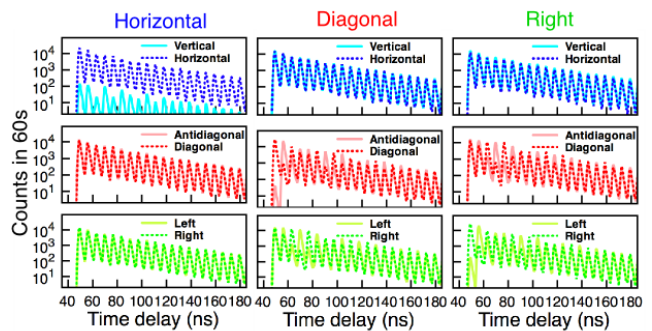


FIG. 6: (Color online) Typical acquisition runs, with a sequence of peaks each corresponding to a cavity round-trip, is shown for a *horizontal*, *diagonal*, and *right* polarization input states. The interval between adjacent peaks amounts to 6.80 ns, in agreement with the given cavity-length. The three plots correspond to the measurements in the bases, from the top, \mathbb{Z} , \mathbb{X} and \mathbb{Y} , respectively. It is worth to note that for the horizontal polarization input state the vertical contribution is negligible and the outputs in the \mathbb{X} and \mathbb{Y} are balanced, as expected for an eigenstate of the cavity unitary evolution.

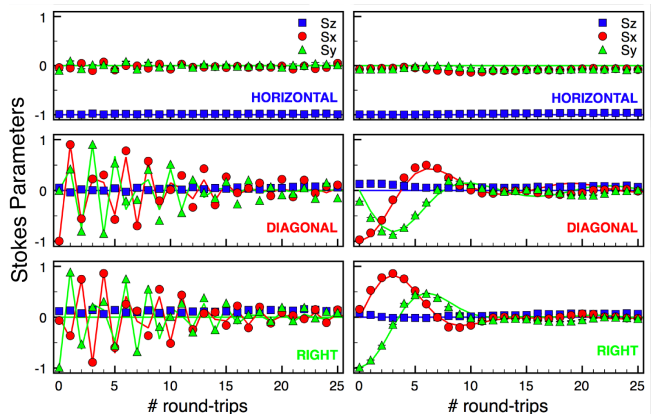


FIG. 7: (Color online) Stokes' parameters as a function of the number of round-trips of the cavity, for *horizontal*, *diagonal*, and *right* polarization input states: (left) only cavity; (right) cavity with a \mathbb{Z} wave-plate in a long arm in order to compensate for the spherical mirror \mathbb{Z} transformation, as shown in Fig. 5. Note how the wave-plate inserted in a long arm of the cavity cancels the polarization-flip for diagonal and right polarization input states due to the spherical mirror transformation. The wave-plate has no effect instead in the case of a horizontal polarization input state, which is an eigenstate of the cavity transformation in both cases. The lines following the experimental data are evaluated by means of a numerical simulation with two fitting parameters: the standard deviation of the Gaussian measure $\sigma_\phi^{\text{est}} = 8.39 \times 10^{-2}$ rad, and the phase difference for horizontal and vertical polarization, $\phi_0 = -0.2182$ rad.

approximation, the phase shift is a linear function of the frequency, $\phi \simeq \phi_0 + \tau\omega$. The integral can be therefore transformed into an average over a Gaussian measure, $d\mu_\phi$, with standard deviation $\sigma_\phi = \tau\sigma_\omega$. The linear passive optical elements constituting the cavity (mirrors and

wave-plates) have been modeled by 2×2 unitary matrices, and the n -th round-trip polarization density matrix has been evaluated by the average over a Monte-Carlo simulation of the measure $d\mu_\phi$ of the n -th power of the matrix describing the effect of a cavity round-trip. The lines fitting the experimental data in Fig. 7 and following, are the numerical fit with two parameters: the standard deviation of the Gaussian measure σ_ϕ^{est} , and the phase difference between horizontal and vertical polarization, ϕ_0 .

D. Polarization decay from the cavity

In order to understand the polarization decoherence caused by cavity round-trips, we have first studied the *cavity only* configuration as shown in Figs. 4 and 5. To quantify the decoherence, we use both purity

$$\mathcal{P} = \text{Tr}(\rho_{\text{out}}^2), \quad (35)$$

and fidelity

$$\mathcal{F} = {}_{in}\langle \pi | \rho_{\text{out}} | \pi \rangle_{in}, \quad (36)$$

where ρ_{out} is the output density matrix and $|\pi\rangle_{in}$ is the pure input polarization state. Purity \mathcal{P} is maximum and equal to one for pure states and to $1/d$ for maximally mixed states of dimension d . Fidelity \mathcal{F} measures the distance between quantum states and the definition of Eq. (36) is valid in the case of the distance between a mixed and a pure state. For two density matrices ρ, σ it is generalized to $F(\rho, \sigma) = (\text{tr} \sqrt{\sqrt{\rho} \sigma \sqrt{\rho}})^2$ [45]. However, one can adopt the alternative definition $F'(\rho, \sigma) = \text{tr} \sqrt{\sqrt{\rho} \sigma \sqrt{\rho}}$ [46], sometimes denoted as \sqrt{F} and called square root fidelity.

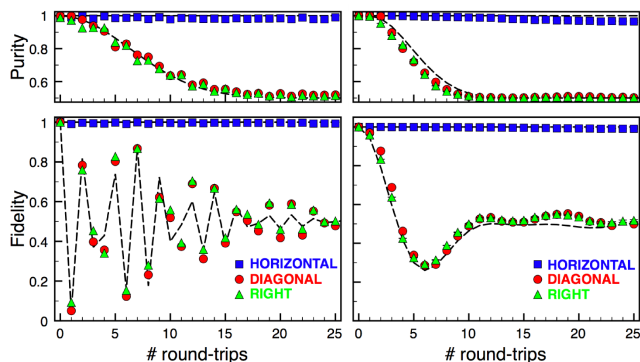


FIG. 8: (Color online) Purity and fidelity versus the number of round-trips for three different input polarization states: left) only cavity; right) cavity with a \mathbb{Z} in a long arm in order to compensate for the spherical mirror \mathbb{Z} transformation, as shown in Fig. 5. *Horizontal* polarization is well preserved. On the contrary the *diagonal* and *right* states quickly decay to the fully mixed state (purity and fidelity equal to $1/2$). Dashed lines curves are obtained by numerical simulation with the same parameters of the previous figure.

The purity and fidelity after each cavity round trip, evaluated from the experimentally reconstructed density matrices, are shown on the left panels in Fig. 8. As expected, the cavity preserves the purity and fidelity only for H polarization input, while for D and R input states, they both quickly decay to the fully mixed state ($\mathcal{P} = \mathcal{F} = 1/2$). Assuming the amplitude spectrum of Eq. (34), it is possible to derive analytically a Gaussian decay of the purity as a function of the number of round-trips n ,

$$\mathcal{P} = \frac{1}{2}[1 + \exp(-2n^2\sigma_\phi^2)]. \quad (37)$$

The standard deviation of the Gaussian distribution of the phase-shift, σ_ϕ , is estimated by a best fit on the experimental data of the purity reported in the left panel of Fig. 8 using the expression of Eq. (37). The obtained value agrees with the estimated parameter from the numerical simulation and it is given by $\sigma_\phi^{\text{est}} = 8.39 \times 10^{-2}$ rad. Differently from the purity, the fidelity depends upon both σ_ϕ and the parameter ϕ_0 , which is the phase difference between H and V polarization reflection at the central frequency ω_0 , as highlighted by the slowly-varying envelope of the fidelity shown in Fig. 8. The flips of the fidelity every round-trip for D and R input polarization state, shown in the left panel of Fig. 8, are instead due to the spherical mirror transformation \mathbb{Z} . The dashed lines following the purity and fidelity data reported in Fig. 8 represent the numerical fit corresponding to the values $\sigma_\phi^{\text{est}} = 8.39 \times 10^{-2}$ rad and $\phi_0 = -0.2182$ rad.

E. Compensating the spherical mirror

In a single round trip the polarization qubit encounters two decohering elements (the two plane mirrors represented by $\mathbb{M}(\omega)$), and a \mathbb{Z} transformation due to the spherical mirror. As shown by Eq. (32), the transformation of the polarization qubit realized by a cavity round-trip is given by the product of a phase-shift $\exp\{-i2\phi(\omega)\mathbb{Z}\}$, with Gaussian-distributed random phase, and a \mathbb{Z} operation, which flips every round trip the D and R polarization, as elucidated by the data reported in the left panels of Figs. 7, and 8. In order to compensate these \mathbb{Z} -flips, we have inserted in one of the long arms of the cavity, before the spherical mirror, an additional wave-plate set to realize a further \mathbb{Z} operation, as shown in Fig. 5. With this new optical element in the setup, the evolution of the polarization state after a round-trip is given by

$$\begin{aligned} \mathbb{U}[\phi(\omega)] &= \mathbb{Z} \cdot \mathbb{Z} \cdot \mathbb{M}_{\mathbb{Z}}(\omega) \cdot \mathbb{M}_{\mathbb{Z}}(\omega) \\ &= \exp\{-i2\phi(\omega)\mathbb{Z}\}. \end{aligned} \quad (38)$$

The behavior of purity and fidelity in this new configuration is shown in the right panels of Fig. 8. The flips in the fidelity decay are now completely eliminated and only the slowly-varying envelop due to ϕ_0 is left. As shown in

the right panels of Fig. 7, also the flips in the Stokes' parameters for D and R input polarizations are eliminated in the new cavity configuration.

IV. BANG-BANG DECOUPLING

Here we experimentally demonstrate the application of BB dynamical decoupling for suppressing decoherence on single-photon polarization qubits flying in the cavity. Polarization decoherence takes place in localized spatial regions (mirrors, S-B, ...), and the BB controls will be implemented in space rather than in time by placing wave-plates along the photon path.

A. Suppressing polarization decoherence of the ring cavity

The BB Pauli group dynamical decoupling is realized by adding two control operations within the cavity: i) a second \mathbb{Z} wave-plate in the long arm of the cavity in addition to the one used for compensating the spherical mirror; ii) a S-B with axis at 45° with respect to the cavity plane and delay equal to $\lambda/2$ in the short arm of the cavity, acting therefore as \mathbb{X} (see Fig. 9). The two

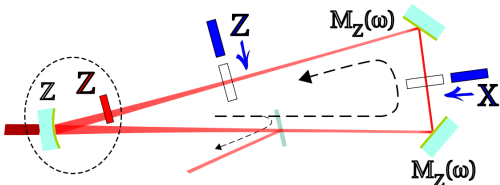


FIG. 9: (Color online) Schematics of the triangular-ring cavity in the presence of BB Pauli group decoupling. An additional \mathbb{Z} wave-plate is inserted in the long arm of the cavity, while a S-B with axis at 45° with respect to the cavity plane and delay equal to $\lambda/2$ is placed in the short arm of the cavity, acting therefore as \mathbb{X} .

controls implement every two cavity round-trips the full Pauli-group decoupling for a polarization qubit [21, 33], and the overall transformation for a double round-trip is given by

$$\begin{aligned} U[\phi(\omega)] &= [\mathbb{Z}M_Z\mathbb{X}M_Z] \cdot [\mathbb{Z}M_Z\mathbb{X}M_Z] \\ &= [\mathbb{Z}\mathbb{X}] [\mathbb{Z}\mathbb{X}] = (iY)^2 = -\mathbb{I}, \end{aligned} \quad (39)$$

where we have omitted the frequency dependence of $M_Z(\omega)$. Therefore the polarization transformation is proportional to the identity operator, thus implying a *perfect* preservation of every input polarization state, i.e., a complete suppression of decoherence. This is experimentally verified for H, D and R input polarizations in Fig. 10, where the purity \mathcal{P} and the fidelity \mathcal{F} of the output polarization state are plotted versus the number of double

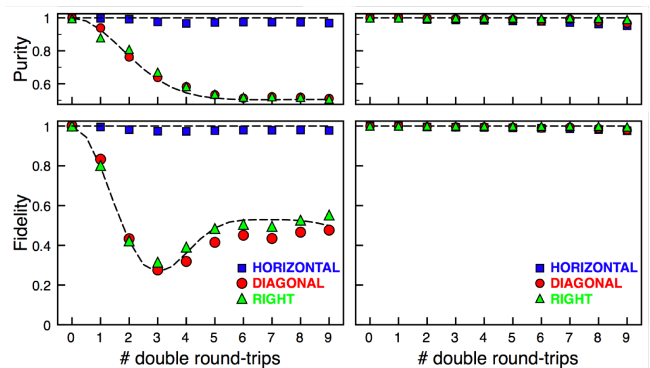


FIG. 10: (Color online) Purity and fidelity as a function of the number of double round trips for three different input polarization states: left) cavity with \mathbb{Z} for compensating the mirror transformation; right) cavity with a \mathbb{X} in the short arm, and a second \mathbb{Z} , as shown in Fig. 11, for implementing the Pauli-group decoupling on the polarization-qubits. The dashed lines represent numerical simulation with the same parameters of the previous figures. (Adapted from Ref. [27]).

round-trips. As we have seen in the previous Section, when BB is not performed (left panels of Fig. 10), polarizations D and R decay to the fully unpolarized state ($\mathcal{P} = \mathcal{F} = 1/2$), while H, being an eigenstate of \mathbb{Z} , is unaffected by decoherence. On the contrary, polarization decoherence is completely suppressed when BB is applied (right panels of Fig. 10).

1. Carr-Purcell decoupling

Polarization decoherence caused by a cavity round-trip acts along a known axis of the Bloch sphere, the z -axis, and therefore even the simplest Carr-Purcell decoupling scheme, based on the decoupling group $\mathcal{G} = \{\mathbb{I}, \mathbb{X}\}$, suffices for suppressing decoherence. We have verified this fact by inserting *only* the \mathbb{X} operation in the short arm of the cavity, by properly adjusting the S-B (see Fig. 11). The Carr-Purcell decoupling scheme requires

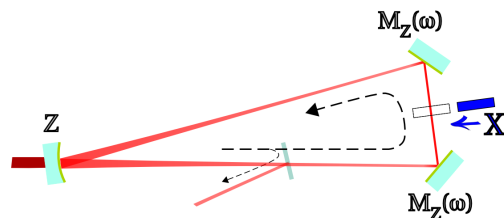


FIG. 11: (Color online) Schematics of the triangular-ring cavity with a wave-plate inserted in the short arm of the cavity, which implements the \mathbb{X} operation in order to realize the Carr-Purcell decoupling scheme for polarization-qubit.

again a double round-trip in the cavity, which gives the

evolution

$$\mathbb{U}[\phi(\omega)] = \mathbb{Z}\mathbb{M}_Z \cdot \mathbb{X} \cdot \mathbb{M}_Z\mathbb{Z}\mathbb{M}_Z \cdot \mathbb{X} \cdot \mathbb{M}_Z = -\mathbb{I}. \quad (40)$$

The polarization transformation is again proportional to the identity operator, implying a perfect preservation of every input polarization state. In fact, when the effective noise acts along a *known* axis, a complete suppression of decoherence is already obtained by employing only *one* Pauli operator, the one realizing a spin-flip around an axis *orthogonal* to the axis of decoherence. This is very well shown in Fig. 12 where, starting from input polarization states H, D and R, the purity \mathcal{P} and the fidelity \mathcal{F} of the output polarization state, with (right panels) and without (left panels) Carr-Purcell decoupling are plotted versus the number of double round-trips.

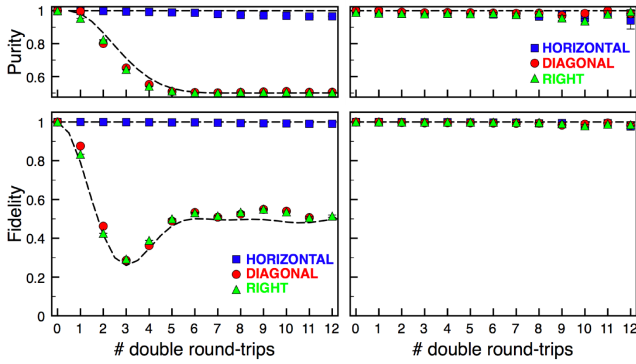


FIG. 12: (Color online) Purity and fidelity versus the number of double round-trips for three different input polarization states: left) only cavity; right) cavity with a \mathbb{X} in the short arm, as shown in Fig. 11, in order to realize the Carr-Purcell decoupling on polarization-qubits affected only by phase-noise along the z -axis. The dashed lines represent numerical simulation with the same parameters of the previous figures.

B. Pauli-group decoupling for the most general polarization decoherence

In the ring-cavity setup, the V and H polarization states are eigenstates of the interaction Hamiltonian of the polarization qubit with its effective environment and are therefore the “pointer states” unaffected by decoherence [1]. In the pointer states basis, decoherence affects only the off-diagonal elements of the polarization density matrix. In the most general case instead, the direction of the pointer state basis in the Bloch–Poincaré sphere is *unknown*. As a consequence in a generic basis, decoherence acts *both* on diagonal and off-diagonal elements of the polarization density matrix. To implement such a generic noise model we have placed in front of each plane mirror a S–B with axis at 45° with respect to the cavity plane (see Fig. 13). The action of the S–B on the polarization state is described by

$$\mathbb{B}_X[\theta] = \exp[-i\theta\mathbb{X}/2], \quad (41)$$

where $\mathbb{X} = |H\rangle\langle V| + |V\rangle\langle H|$, and θ is the noise delay-phase. The S–B together with a plane mirror are described by the operator

$$\mathbb{N}(\omega, \theta) = \mathbb{M}_Z(\omega)\mathbb{B}_X(\theta). \quad (42)$$

The transformation of the polarization state after two round-trips in the presence of the S–Bs is therefore given by

$$\mathbb{U}_{fe}[\phi(\omega), \theta] = [\mathbb{N}(\omega, \theta)\mathbb{N}(\omega, \theta)] \cdot [\mathbb{N}(\omega, \theta)\mathbb{N}(\omega, \theta)]. \quad (43)$$

The free evolution (*fe*) operator $\mathbb{U}_{fe}[\phi(\omega), \theta]$ can be rewritten as

$$\mathbb{U}_{fe}[\phi(\omega), \theta] = \exp[-i\alpha_{fe}(\omega, \theta) \vec{s}_{fe}(\omega, \theta) \cdot \vec{\sigma}], \quad (44)$$

which describes a rotation in the Bloch–Poincaré sphere of an angle $2\alpha_{fe}(\omega, \theta)$ around the direction individuated by $\vec{s}_{fe}(\omega, \theta)$. Therefore by varying θ and the bandwidth of radiation spectrum, i.e. the distribution of ϕ , one implements the generic polarization decoherence. The rotation angle is given by the implicit expression

$$\sin[\alpha_{fe}(\omega, \theta)/2] = \sin[\phi(\omega)/2] \cos(\theta/2), \quad (45)$$

and

$$\vec{s}_{fe}(\omega, \theta) = \frac{1}{2 \sin \alpha_{fe}(\omega, \theta)} \left\{ \begin{aligned} &\sin \theta [\cos \phi(\omega) - 1], \\ &\sin \theta \sin \phi(\omega), \\ &(1 + \cos \theta) \sin \phi(\omega) \end{aligned} \right\}. \quad (46)$$

Pauli-group decoupling is again realized every two-round trips by adding the BB operations \mathbb{X} (implemented by adding to the noise phase-delay θ of the S–B present in the short arm of the cavity, a further delay of $\lambda/2$) and \mathbb{Z} in the cavity [21, 33] as shown in Fig. 13. The over-

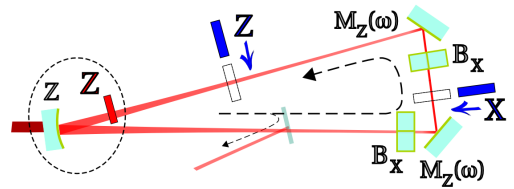


FIG. 13: (Color online) Schematics of the experimental apparatus for generic noise.

all transformation after the two round-trips for a given frequency component is now given by

$$\mathbb{U}_{bb}[\phi(\omega), \theta] = [\mathbb{Z}\mathbb{N}(\omega, \theta)\mathbb{X}\mathbb{N}(\omega, \theta)] \cdot [\mathbb{Z}\mathbb{N}(\omega, \theta)\mathbb{X}\mathbb{N}(\omega, \theta)], \quad (47)$$

which can be rewritten, as in the free evolution case, as a rotation in the Bloch–Poincaré sphere,

$$\mathbb{U}_{bb}[\phi(\omega), \theta] = \exp[-i\alpha_{bb}(\omega, \theta) \vec{s}_{bb}(\omega, \theta) \cdot \vec{\sigma}], \quad (48)$$

with

$$\cos \alpha_{bb}(\omega, \theta) = -(\sin \phi(\omega) \sin \theta)/2, \quad (49)$$

and

$$\begin{aligned} \vec{s}_{bb}(\omega, \theta) = \{ & -\sin \phi(\omega) \sin^2(\theta/2), \\ & 1 - 2 \sin^2(\theta/2) \sin^2[\phi(\omega)/2], \\ & -\sin \theta \sin^2[\phi(\omega)/2] \} / [\sin \alpha_{bb}(\omega, \theta)]. \quad (50) \end{aligned}$$

1. Suppressing decoherence of an input elliptical polarization state

We have performed a first test of the ability of Pauli group decoupling for controlling decoherence under generic noise, by injecting in the cavity an elliptical polarization state, corresponding to an equal-weighted superposition of V, A (*anti-diagonal*) and R polarizations (see the experimentally reconstructed density matrix and Bloch-Poincaré sphere representation in Fig. 14). In case of no BB control, the resulting fast polarization decay of the purity, as a function of the number of double round-trips, is shown in the left panel of Fig. 14, for different noise delay-phases θ . The recovery of purity after the application of BB is evident from the right panel of the Fig. 14.

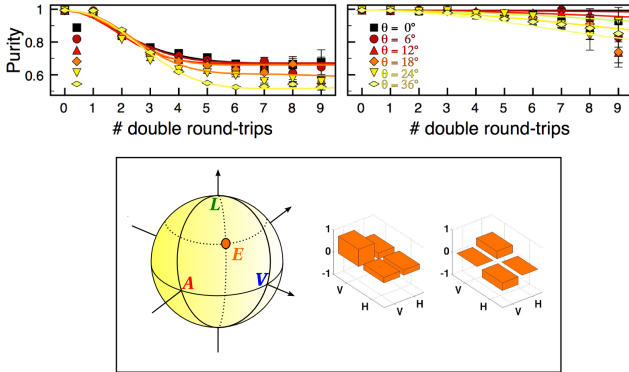


FIG. 14: (Color online) Purity as a function of the number of double round trips for different values of the noise delay-phase θ for an elliptical polarization input state. The lines represent numerical simulation with the parameters of the previous figures. Inset: real and imaginary parts of the density matrix of the elliptical polarization input state, also shown on the Bloch-Poincaré sphere as the point labeled E . (Adapted from Ref. [47]).

2. Purity and fidelity averaged over the Bloch-Poincaré sphere

The experiment with the input elliptical polarization state already shows the effectiveness of the BB Pauli group decoupling for suppressing decoherence. However,

in order to be useful for any quantum information application, the scheme must work for every input polarization. Therefore, in order to better highlight the usefulness of BB decoupling to combat generic birefringence-induced decoherence, we have studied the evolution of the purity and the fidelity, averaging the input state over the whole Bloch-Poincaré sphere, both with (right panels of Fig. 15) and without BB decoupling (left panels of Fig. 15). Each curve corresponds to a different orientation of the noise delay-phase θ of the S-B. BB again inhibits decoherence because, for each orientation of the decoherence-axis, both the average purity and the average fidelity in the presence of BB are significantly higher than the corresponding value without BB. The curve for $\theta = 0$ reproduces the almost perfect preservation of the previous experiment of Sec. IVA. Instead polarization protection progressively worsens for increasing values of θ . When θ is varied, the properties of the effective environment of the polarization qubit associated with the effective birefringence caused by the mirrors changes in a nontrivial way, but a simple analytical explanation of the result can be given when the pulses are not too broad in frequency.

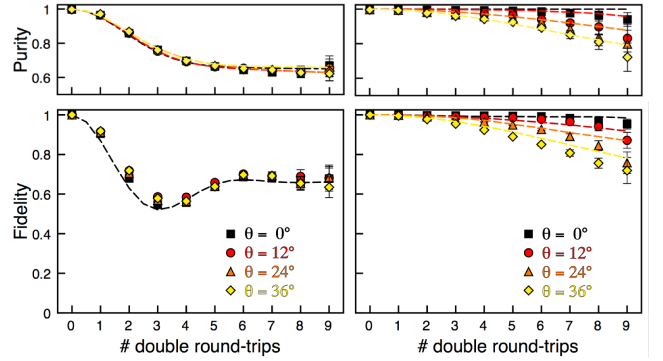


FIG. 15: (Color online) Average purity and fidelity as a function of the number of double round trips for different values of the generic noise phase-delay parameter, θ : left) without bang-bang control: right) when applied the bang-bang control. The lines represent numerical simulation with the parameters of the previous figures. (Adapted from Ref. [27]).

3. Analytical explanation of the results

An approximate analytical description of the evolution of the polarization state as it circles within the cavity can be given under the assumption that the pulse is not too broad in frequency, $\sigma_\phi \ll \pi$, which is well verified in the present experiment. In this case, α_j and \vec{s}_j ($j = fe, bb$) do not vary appreciably over the range of relevant phase shifts ϕ and one can approximate $\vec{s}_j(\phi)$ with its value at the pulse center $\vec{s}_j(\phi_0)$, while $\alpha_j(\phi)$ can be approximated by its second-order expansion around ϕ_0 ,

$$\alpha(\phi) \simeq \alpha_0 + \dot{\alpha}_0(\phi - \phi_0) + \frac{1}{2}\ddot{\alpha}_0(\phi - \phi_0)^2. \quad (51)$$

After lengthy but straightforward calculations, one gets for the output Bloch vector \vec{P}_{out} , which determines completely the density matrix as expressed in Eq. (22),

$$\vec{P}_{out} = V^{(n)} \vec{P}_{in}. \quad (52)$$

The matrix $V^{(n)}$ is given by

$$V_{ij}^{(n)} = \mathcal{D}_n O_{ij}^{(n)} + (1 - \mathcal{D}_n) s(\phi_0)_i s(\phi_0)_j \quad (53)$$

($i, j = x, y, z$), where the ‘‘decoherence factor’’ \mathcal{D}_n is given by

$$\mathcal{D}_n = [1 + n^2 \ddot{\alpha}_0^2 \sigma_\phi^4]^{-1/4} \exp \left[-\frac{n^2 \dot{\alpha}_0^2 \sigma_\phi^2}{1 + n^2 \ddot{\alpha}_0^2 \sigma_\phi^4} \right], \quad (54)$$

and the matrix

$$\begin{aligned} O_{ij}^{(n)} &= \delta_{ij} \cos 2n\gamma_n \\ &+ s(\phi_0)_i s(\phi_0)_j (1 - \cos 2n\gamma_n) \\ &- \varepsilon_{ijk} s(\phi_0)_k \sin 2n\gamma_n \end{aligned} \quad (55)$$

is the orthogonal matrix describing the rotation around the $\vec{s}(\phi_0)$ -axis of an angle $2\gamma_n$, with

$$\gamma_n = \alpha_0 + \frac{1}{2} \frac{n^2 \ddot{\alpha}_0 \dot{\alpha}_0^2 \sigma_\phi^2}{1 + n^2 \ddot{\alpha}_0^2 \sigma_\phi^4} + \frac{1}{4n} \arctan(n \ddot{\alpha}_0 \sigma_\phi^2). \quad (56)$$

The output purity and fidelity are respectively given by

$$\begin{aligned} \mathcal{P}_n &= \frac{1}{2} (1 + \vec{P}_{out} \cdot \vec{P}_{out}) \\ &= \frac{1}{2} \left\{ 1 + 2\mathcal{D}_n (1 - \mathcal{D}_n) [\vec{P}_{in} \cdot \vec{s}(\phi_0)] [\vec{P}(\gamma_n) \cdot \vec{s}(\phi_0)] \right. \\ &\quad \left. + \mathcal{D}_n^2 + (1 - \mathcal{D}_n)^2 [\vec{P}_{in} \cdot \vec{s}(\phi_0)]^2 \right\}, \end{aligned} \quad (57)$$

and

$$\begin{aligned} \mathcal{F}_n &= \frac{1}{2} (1 + \vec{P}_{in} \cdot \vec{P}_{out}) \\ &= \frac{1}{2} \left\{ 1 + \mathcal{D}_n \vec{P}_{in} \cdot \vec{P}(\gamma_n) + (1 - \mathcal{D}_n) [\vec{P}_{in} \cdot \vec{s}(\phi_0)]^2 \right\}, \end{aligned} \quad (58)$$

with $\vec{P}(\gamma_n) = O^{(n)} \vec{P}_{in}$. These expressions are general and apply both to the BB case as well to the one without BB. The two cases differ only in the explicit expressions of $\vec{s}(\phi_0)$, α_0 , $\dot{\alpha}_0$, and $\ddot{\alpha}_0$. Since $\lim_{n \rightarrow \infty} \mathcal{D}_n = 0$, fidelity and purity tend asymptotically to the same limit

$$\mathcal{P}_\infty = \mathcal{F}_\infty = \frac{1}{2} \{1 + [\vec{P}_{in} \cdot \vec{s}(\phi_0)]^2\}. \quad (59)$$

This asymptotic situation corresponds to the existence of a pointer basis [1] (analogous to the principal states of polarization in fibers [37]), formed by the two states with Bloch vector equal to $\pm \vec{s}(\phi_0)$, which are unaffected by decoherence. All the other polarization states instead decohere, with maximum decoherence for the states on

the plane orthogonal to $\vec{s}(\phi_0)$. As a consequence, when averaged over the initial state, purity and fidelity tends to 2/3. In the $n \rightarrow \infty$ regime, BB and no-BB case differ only in the direction $\vec{s}(\phi_0)$ of the pointer basis and therefore BB is not advantageous with respect to the no-BB case in this regime.

However, the interesting regime of our experiment is the one corresponding to a small round-trip number n . In that regime our ring-cavity well mimics a portion of a one-way quantum communication channel with constant dispersive properties, like a small portion of an optical fiber. For small n one has

$$\begin{aligned} 1 - \mathcal{F} &\simeq (1 - \mathcal{P})/2 \\ &\simeq n^2 [\dot{\alpha}_j^0 \sigma_\phi]^2 \{1 - [\vec{P}_{in} \cdot \vec{s}_j(\phi_0)]^2\}/2, \end{aligned} \quad (60)$$

with $j = \{fe, bb\}$, showing that the smaller $\dot{\alpha}^0$ the better the decoherence suppression. BB Pauli-group decoupling acts just by decreasing $|\dot{\alpha}^0|$: by using Eqs. (45)-(49) and the fact that ϕ_0 is quite small in our experiment, one gets $\dot{\alpha}_{fe}^0 \simeq \cos(\theta/2)$, $\dot{\alpha}_{bb}^0 \simeq \sin(\theta/2) \cos(\theta/2)$, showing that it is always $\dot{\alpha}_{fe}^0 > \dot{\alpha}_{bb}^0$ and therefore that BB better preserves the polarization qubit for any orientation of the decoherence axis, confirming its applicability to optical fibers polarization control. These expressions also explain the perfect preservation of the polarization qubit of Fig. 10: the latter refers to $\theta = 0$, implying $\dot{\alpha}_{fe}^0 = 1$ and $\dot{\alpha}_{bb}^0 = 0$.

V. CONCLUSIONS

We have presented the details of the experiment of Ref. [27], which showed how BB dynamical decoupling can be efficiently implemented in the optical domain in order to suppress the polarization decoherence caused by the propagation of light pulses within birefringent media. In such media, the optical properties depend upon both frequency and polarization and the frequency degree of freedom acts as an effective environment on the photon polarization. With photons BB dynamical decoupling can be realized by placing appropriate optical elements (i.e., wave-plates) implementing suitable unitary operations along the photon path. In the present proof-of-principle demonstration, a one-way communication channel is mimicked by a ring-cavity, in which an effective birefringence is introduced by two mirrors at 45 degrees whose reflectivity is responsible for the decay of the density matrix off-diagonal elements, in the basis formed by H and V polarizations. In a first experiment, BB dynamical decoupling was shown to be able to perfectly suppress this kind of decoherence. In a second experiment, we modified the setup by placing two Soleil-Babinet compensators in front of the mirrors. This allowed us to simulate the most general model of decoherence, for which the pointer basis is unknown. Also in this case the Pauli group BB decoupling was able to significantly reduce decoherence, as predicted by [11].

Several elements suggest that our experiment is significant for the potential extension of BB decoupling to the dynamics of polarization pulses propagating in optical fibers. First, the interaction Hamiltonian governing the dynamics in the ring cavity is strictly related to the one causing PMD in optical fibers [21]. Second, the one-way nature of the ring cavity well mimics a fiber-based communication channel. Third, the optical elements introducing decoherence in the ring-cavity doubtless realize a worst-case version of the fiber dynamics, because the errors they introduce accumulate systematically while in a fiber they are distributed at random.

We plan to experimentally investigate the optimal

length for placing the BB operations along an SM fiber, obtained from a tradeoff between the two opposite requests of minimizing the attenuation of the fiber and maximizing the decoherence suppression.

VI. ACKNOWLEDGMENTS

We acknowledge the funding of the EC project FP6-IP-QAP. M.L. is supported by the 5% grant C.F. 81001910439.

-
- [1] W. H. Zurek, *Rev. Mod. Phys.* **75**, 715 (2003).
 [2] P. W. Shor, *Phys. Rev. A* **52**, R2493 (1995).
 [3] A. M. Steane, *Nature* **399**, 124 (1999).
 [4] J. Chiaverini, D. Leibfried, T. Schaetz, M. D. Barrett, R. B. Blakestad, J. Britton, W. M. Itano, J. D. Jost, E. Knill, C. Langer, et al., *Nature* **432**, 602 (2004).
 [5] N. Boulant, L. Viola, E. M. Fortunato, and D. G. Cory, *Physical Review Letters* **94**, 130501 (pages 4) (2005).
 [6] P. Zanardi and M. Rasetti, *Phys. Rev. Lett.* **79**, 3306 (1997).
 [7] D. Kielpinski, V. Meyer, M. A. Rowe, C. A. Sackett, W. M. Itano, C. Monroe, and D. J. Wineland, *Science* **291**, 1013 (2001).
 [8] R. Prevedel, M. S. Tame, A. Stefanov, M. Paternostro, M. S. Kim, and A. Zeilinger, *Physical Review Letters* **99**, 250503 (pages 4) (2007).
 [9] D. Vitali, P. Tombesi, and G. J. Milburn, *Phys. Rev. Lett.* **79**, 2442 (1997).
 [10] L. Viola and S. Lloyd, *Physical Review A* **58**, 2733 (1998).
 [11] L. Viola, S. Lloyd, and E. Knill, *Phys. Rev. Lett.* **83**, 4888 (1999).
 [12] D. Vitali and P. Tombesi, *Phys. Rev. A* **59**, 4178 (1999).
 [13] P. Zanardi, *Physics Letters A* **258**, 77 (1999).
 [14] A. G. Kofman and G. Kurizki, *Phys. Rev. Lett.* **93**, 130406 (2004).
 [15] P. Facchi, S. Tasaki, S. Pascazio, H. Nakazato, A. Tokuse, and D. A. Lidar, *Physical Review A (Atomic, Molecular, and Optical Physics)* **71**, 022302 (pages 22) (2005).
 [16] R. Ernst, G. Bodenhausen, and A. Wokaun, *Principles of Nuclear Magnetic Resonance in One and Two Dimensions* (Clarendon Press, Oxford, 1987).
 [17] G. S. Agarwal, M. O. Scully, and H. Walther, *Phys. Rev. Lett.* **86**, 4271 (2001).
 [18] C. Search and P. R. Berman, *Phys. Rev. Lett.* **85**, 2272 (2000).
 [19] D. Vitali and P. Tombesi, *Phys. Rev. A* **65**, 012305 (2001).
 [20] L.-A. Wu and D. A. Lidar, *Physical Review A (Atomic, Molecular, and Optical Physics)* **70**, 062310 (pages 8) (2004).
 [21] S. Massar and S. Popescu, *New Journal of Physics* **9**, 158 (2007).
 [22] L. Viola, E. M. Fortunato, M. A. Pravia, E. Knill, R. Laflamme, and D. G. Cory, *Science* **293**, 2059 (2001).
 [23] J. J. L. Morton, A. M. Tyryshkin, A. Ardavan, S. C. Benjamin, K. Porfyakis, S. A. Lyon, and G. A. D. Briggs, *Nature Physics* **2**, 40 (2006).
 [24] E. Fraval, M. J. Sellars, and J. J. Longdell, *Physical Review Letters* **95**, 030506 (2005).
 [25] M. J. Biercuk, H. Uys, A. P. VanDevender, N. Shiga, W. M. Itano, and J. J. Bollinger, *Nature* **458**, 996 (2009).
 [26] A. Berglund, *quant-ph/0010001* (2000).
 [27] S. Damodarapur, M. Lucamarini, G. D. Giuseppe, D. Vitali, and P. Tombesi, *Phys. Rev. Lett.* **103**, 040502 (2009).
 [28] N. Gisin and R. Thew, *Nat Photon* **1**, 165 (2007).
 [29] M. Martinelli, *Opt. Commun.* **72**, 341 (1989).
 [30] L. M. K. Vandersypen and I. L. Chuang, *Rev. Mod. Phys.* **76**, 1037 (2005).
 [31] E. L. Hahn, *Phys. Rev.* **80**, 580 (1950).
 [32] H. Y. Carr and E. M. Purcell, *Phys. Rev.* **94**, 630 (1954).
 [33] L. Viola, E. Knill, and S. Lloyd, *Phys. Rev. Lett.* **82**, 2417 (1999).
 [34] L. Viola, *Journal of Modern Optics* **51**, 2357 (2004).
 [35] L.-M. Duan and G.-C. Guo, *Physics Letters A* **261**, 139 (1999).
 [36] L. Viola and E. Knill, *Physical Review Letters* **94**, 060502 (pages 4) (2005).
 [37] C. D. Poole, *Opt. Lett.* **13**, 687 (1988).
 [38] A. Galtarossa, M. S., L. Palmieri, and T. Tambosso, *Optics Letters* **25**, 384 (2000).
 [39] N. Gisin, G. Ribordy, W. Tittel, and H. Zbinden, *Rev. Mod. Phys.* **74**, 145 (2002).
 [40] A. J. Barlow, J. J. Ramskov-Hansen, and D. N. Payne, *Applied Optics* **20**, 2962 (1981).
 [41] D. F. V. James, P. G. Kwiat, W. J. Munro, and A. G. White, *Phys. Rev. A* **64**, 052312 (2001).
 [42] R. M. A. Azzam and N. M. Bashara, *Ellipsometry and Polarized Light* (North-Holland, Amsterdam, 1977).
 [43] E. Brinkmeyer, *Opt. Lett.* **6**, 575 (1981).
 [44] B. E. A. Saleh and M. C. Teich, *Fundamentals of Photonics* (Wiley, New York, 1991).
 [45] R. Jozsa, *Journal of Modern Optics* **41**, 2315 (1994).
 [46] M. A. Nielsen and I. L. Chuang, *Quantum Computation and Quantum Information* (Cambridge University Press, Cambridge, England, 2000).
 [47] S. Damodarapur, M. Lucamarini, G. D. Giuseppe, D. Vitali, and P. Tombesi, *SPIE Newsroom – Optoelectronics & Optical Communications* (29 April 2009).